Reprints of the Published papers

Effect of breakup processes on the near-barrier elastic scattering of the ^{6,7}Li + ^{232}Th systems

Shradha Dubey,[1,2] S. Mukherjee,[1] D. C. Biswas,[2,*] B. K. Nayak,[2] D. Patel,[1] G. K. Prajapati,[2] Y. K. Gupta,[2] B. N. Joshi,[2] L. S. Danu,[2] S. Mukhopadhyay,[2] B. V. John,[2] V. V. Desai,[2] S. V. Suryanarayana,[2] R. P. Vind,[2] N. N. Deshmukh,[1] S. Appnnababu,[1] and P. M. Prajapati[1]

[1]*Physics Department, Faculty of Science, M.S. University of Baroda, Vadodara 390002, India*

[2]*Nuclear Physics Division, Bhabha Atomic Research Centre, Mumbai 400085, India*

(Received 7 August 2013; revised manuscript received 25 November 2013; published 15 January 2014)

Elastic scattering angular distribution measurements of the weakly bound ^{6,7}Li projectiles on a ^{232}Th target have been carried out at different bombarding energies close to the Coulomb barrier. The data have been analyzed for both systems using the optical model ECIS code with phenomenological Woods-Saxon and Sao Paulo double-folding forms of the optical potentials. The energy dependence of the volume-type real and imaginary parts of the optical potentials are derived from the best fit of the experimental angular distribution data. The usual threshold anomaly has been observed for the ^{7}Li + ^{232}Th system, whereas there is an indication of a breakup threshold anomaly in case of the ^{6}Li + ^{232}Th system. Results on total reaction cross sections obtained from the optical model analysis for both systems have been interpreted to understand the role of projectile breakup on the reaction mechanism.

DOI: 10.1103/PhysRevC.89.014610 PACS number(s): 25.70.Bc, 24.10.Ht, 25.70.Mn

I. INTRODUCTION

The study of elastic scattering around the Coulomb barrier is important to determine the energy dependence of potential parameters for the real and the imaginary parts of the nuclear interaction in order to understand the coupling of intrinsic degrees of freedom to the relative motion of the colliding nuclei. From the systematic analysis of elastic scattering measurements involving tightly bound nuclei, a phenomenon called the "threshold anomaly" (TA) has been observed in a number of systems [1–4]. A characteristic localized peak in the real part and the corresponding decrease of the imaginary part of the potential are observed as the bombarding energy decreases below the Coulomb barrier. This has been understood in terms of coupling of the elastic channel to the direct reaction channels that generate an additional attractive real dynamical polarization potential, which results in a decrease of the Coulomb barrier and enhancement of the fusion cross section.

There has been renewed interest in elastic scattering studies using weakly bound projectiles, with the observation of the rapid variation of the optical potential parameters with energies around the Coulomb barrier. The study of the TA has become one of the tools to investigate the influence of the breakup and other reaction mechanisms on the elastic and fusion channels [5]. In the case of elastic scattering for the ^{7}Li projectile on different targets such as ^{59}Co [6], ^{80}Se [7], ^{138}Ba [8], and ^{208}Pb [9], the conventional TA has been identified. In these measurements, an increase in the real part of the potentials at energies around the Coulomb barrier was observed, indicating the presence of the usual TA. The TA situation is not clear in the case of the ^{6}Li projectile, which has no bound excited state and breaks up into $\alpha + d$ at 1.48 MeV, whereas ^{7}Li has one bound excited state at 0.48 MeV and breaks up into $\alpha + t$ at 2.47 MeV. A different type of energy dependence from that of the TA is observed for the scattering of loosely bound projectiles; this has been known as the "breakup threshold anomaly" (BTA) [10,11]. In the case of the BTA, a repulsive polarization potential is generated due to the coupling of breakup channels to the elastic scattering, which causes an increase in the imaginary potential and corresponding decrease in the real part. Several earlier works on the elastic scattering of ^{6}Li on various targets such as ^{27}Al [12], ^{64}Ni [13], ^{64}Zn [14], ^{80}Se [7], ^{90}Zr [15], ^{116,112}Sn [16], ^{138}Ba [8], ^{144}Sm [17],^{208}Pb [9], and ^{209}Bi [18] have indicated that results are compatible with the absence of the conventional TA. In these cases it has been observed that there are small increases in the imaginary part of the optical potential rather than decreasing to zero at energies below the Coulomb barrier, indicating the absence of the normal TA. Contradictory results have been reported for ^{138}Ba [10] and ^{28}Si [19] targets, where the BTA has been observed for both ^{6,7}Li projectiles. However, this observation must be supported by more experimental data. In particular, there is a lack of data with heavy targets, where the strong Coulomb field may induce different behavior than with lighter targets. The motivation of the present work is to investigate the TA and the BTA by elastic scattering measurements using a heavy target (^{232}Th), where the Coulomb effects will be more pronounced. The present data for ^{6,7}Li + ^{232}Th reactions, supported by those available in the literature [5–18], can help to understand the overall trends in the TA and the BTA for loosely bound nuclei.

In the present work, elastic scattering angular distribution measurements have been carried out for ^{6,7}Li + ^{232}Th systems at energies from 25% below the Coulomb barrier ($V_{\rm lab}$ = 32 MeV) to approximately 40% above the barrier. The total reaction cross sections for these systems have also been derived to understand the role of projectile breakup on the total reaction cross sections. The present article has been organized in the following way. The experimental setup is described in Sec. II. Data analyses using both the Wood-Saxon potential (WSP)

*dcbiswas@barc.gov.in

and double-folding Sao Paulo potential (SPP) to determine the energy dependence of potential parameters is discussed in Sec. III. The dispersion relation (DR) analysis is discussed in Sec. IV. In Sec. V, a systematic study of the total reaction cross section for ^{6,7}Li + ^{232}Th systems is discussed. In Sec. VI, a summary and conclusions of the present work are reported.

II. EXPERIMENTAL DETAILS

The experiment was performed at the 14UD BARC-TIFR Pelletron Accelerator Facility at Mumbai using beams of ^{6,7}Li in a wide energy range around the Coulomb barrier, i.e., 24, 26, 30, 32, 35, 40, and 44 MeV for the ^{7}Li + ^{232}Th system and 26, 30, 32, 35, 40, and 44 MeV for the ^{6}Li + ^{232}Th system. The observed uncertainty in the beam energy was about 1% for all the selected energies. A self-supporting 1.6 mg/cm^2 thick ^{232}Th target was placed at the center of the general purpose scattering chamber and the elastically scattered ^{6,7}Li particles were detected by ΔE-E telescopes mounted on a movable arm of the chamber. Four telescopes of thicknesses T_1 with $\Delta E = 25$ μm and $E = 300$ μm, T_2 with $\Delta E = 15$ μm and $E = 1500$ μm, T_3 with $\Delta E = 15$ μm and $E = 1000$ μm, and T_4 with $\Delta E = 15$ μm and $E = 1000$ μm were used in the experiment. The detector telescopes were placed at an angular separation of 10° and two 300-μm-thick monitor detectors were mounted at fixed angles of ±15° with respect to the beam direction for absolute normalization and beam monitoring. The angular distributions were measured in steps of 5° in the angular range from 20° to 170°. The uncertainty on the angular range of each telescope was ±0.68°. A typical bi-parametric ΔE-$E_{\rm res}$ spectrum for the ^{7}Li + ^{232}Th system at $E_{\rm lab} = 44$ MeV and $\theta_{\rm lab} = 60°$ is plotted in Fig. 1, showing the isotopic separation of the reaction products. In the inset of Fig. 1, the projection onto the $E_{\rm res}$ axis for the $Z = 3$ events has been plotted. For angular distribution studies, the area of the elastically scattered peak was obtained at various angles for all energies.

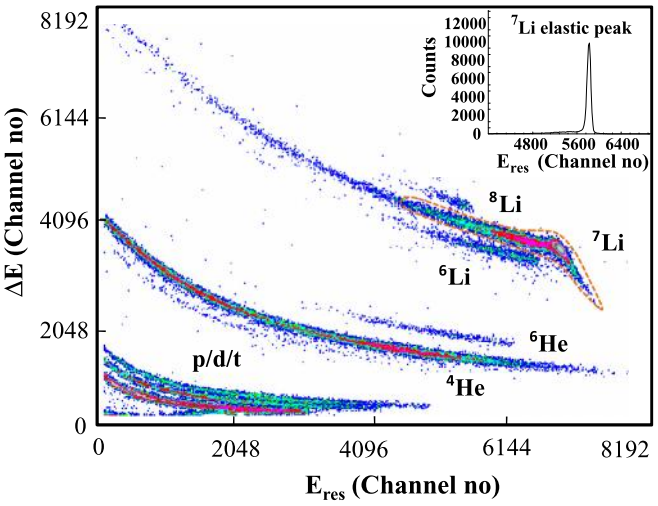

FIG. 1. (Color online) A typical two-dimensional ΔE vs $E_{\rm res}$ spectrum for the ^{7}Li + ^{232}Th system at $E_{\rm lab} = 44$ MeV and $\theta_{\rm lab} = 60°$. The projection of the ^{7}Li elastic peak of the bi-parametric ΔE vs $E_{\rm res}$ spectrum is shown in the inset.

III. OPTICAL MODEL ANALYSIS OF ELASTIC SCATTERING

In this section the procedure for analyzing the elastic scattering angular distribution data is presented. Two different types of optical model potential have been used in order to check whether the results show any dependence on the theoretical models. In Sec. III A the analysis with a phenomenological Woods-Saxon form interaction potential is described, and in Sec. III B the analysis performed by using the double-folding SPP is presented [20,21].

A. Analysis with phenomenological Woods-Saxon potential

The optical model fits to the elastic scattering data have been performed using the ECIS code [22]. The phenomenological Woods-Saxon form of the interaction potential with only volume terms has been used in the analysis. To obtain the starting parameters, a global best-fit procedure for all energies was performed, using the three parameters characterized by the real and imaginary depth of the potential, reduced radii (r_o), and the diffuseness (a_v and a_w). Thereafter, in order to avoid a fit procedure with too many parameters, the real and imaginary reduced radii were fixed at 1.06 fm for both ^{6,7}Li + ^{232}Th systems, which is similar to the value used earlier [16]. This analysis procedure has been successfully adopted in the past by several groups [8,12,13,16,17,19,23]. By using this radius, and varying the diffuseness parameters a_v and a_w (real and imaginary, respectively) within the interval from 0.67 fm to 0.75 fm, an attempt was made to obtain the best possible parameters for the optical potential to describe the elastic scattering angular distribution. In the present work, the best possible fitted values were obtained for a_v, $a_w = 0.71$ fm. The real and imaginary radius parameters ($r_o = 1.06$ fm) and diffuseness parameters (a_v, $a_w = 0.71$ fm) were fixed for all energies. The depths of the real and imaginary potentials were varied to obtain the minimum value of χ^2 for both ^{6,7}Li + ^{232}Th systems. The potential parameter values for the best fit and the total reaction cross section are listed in Table I and Table II for

TABLE I. Optical model parameters obtained by fitting the experimental elastic differential cross section data using the ECIS code (with $a_o = 0.71$ fm and $r_o = 1.06$ fm) and SPP calculations for the ^{7}Li + ^{232}Th system.

$E_{\rm lab}$	Wood Saxon potential				Sao Paulo potential			
(MeV)	V_r (MeV)	V_i (MeV)	$\frac{\chi^2}{n}$	σ_R (mb)	N_R	N_I	$\frac{\chi^2}{n}$	σ_R (mb)
24	70.200	13.70	1.66	0.129	0.81	0.36	1.66	0.114
26	85.000	19.70	1.66	0.919	0.94	0.45	1.57	0.807
30	95.220	30.70	2.72	20.07	1.55	0.55	2.01	18.90
32	360.00	58.54	0.38	260.8	2.00	0.56	0.36	260.6
35	157.90	73.62	1.11	470.7	0.88	0.61	1.19	471.9
40	147.42	78.34	2.73	967.7	0.83	0.60	2.82	959.7
44	115.80	67.66	2.66	1215	0.66	0.53	2.89	1213

TABLE II. Optical model parameters obtained by fitting the experimental elastic differential cross section data using the ECIS code (with $a_o = 0.71$ fm and $r_o = 1.06$ fm) and SPP calculations for the ^{6}Li + ^{232}Th system.

E_{lab}	Wood Saxon potential				Sao Paulo potential			
(MeV)	V_r (MeV)	V_i (MeV)	$\frac{\chi^2}{n}$	σ_R (mb)	N_R	N_I	$\frac{\chi^2}{n}$	σ_R (mb)
26	105.6	90.00	2.33	3.884	0.72	1.06	1.92	3.57
30	263.3	167.7	1.70	105.4	1.41	1.72	2.08	107.0
32	215.9	394.6	2.37	404.4	1.29	3.68	2.64	398.4
35	130.2	183.5	1.02	561.2	0.82	1.52	1.45	550.6
40	97.69	136.0	2.39	970.6	0.87	1.09	2.71	963.6
44	128.8	144.7	0.68	1336	0.80	1.24	0.51	1335

^{7}Li + ^{232}Th and ^{6}Li + ^{232}Th systems, respectively. The best-fit optical model parameters show significant energy dependence as reflected from Table I and Table II, which is a characteristic feature of elastic scattering. Figures 2 and 3 show the best fit of the experimental data for the elastic scattering angular distributions for ^{7}Li + ^{232}Th and ^{6}Li + ^{232}Th systems.

Very good fits to the data were obtained, and expectedly it was found that several families of optical potential describe the angular distributions equally well. To reduce the ambiguities of the best-fitted parameters for the optical potential, the strong sensitive radii R_{Sr} and R_{Si} corresponding to the real and imaginary potential were determined. For this purpose the radius parameters were kept fixed and the depth parameters of the real and imaginary potentials were fitted by varying the diffuseness from 0.67 to 0.75 fm, in steps of 0.02 fm for all the energies of ^{6,7}Li + ^{232}Th systems. The strong sensitive radii [24] were determined by where the real and the imaginary

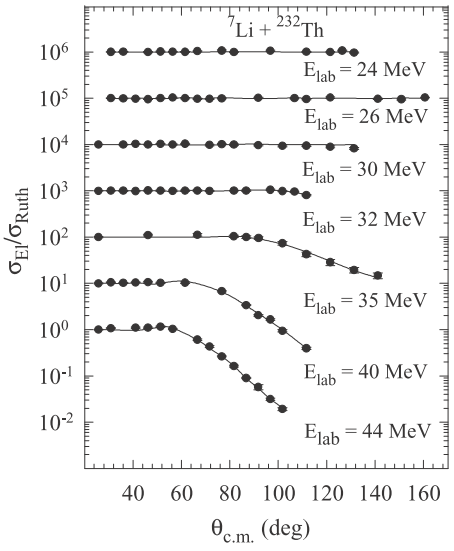

FIG. 2. Experimental elastic scattering cross section (σ_{El}) normalized to the Rutherford cross section (σ_{Ruth}) as a function of $\theta_{c.m.}$ for the ^{7}Li + ^{232}Th system (solid circles) (suitably scaled up for each energy) and their best fits from optical model calculations (solid lines). The curves correspond to the best fits obtained by using the ECIS code.

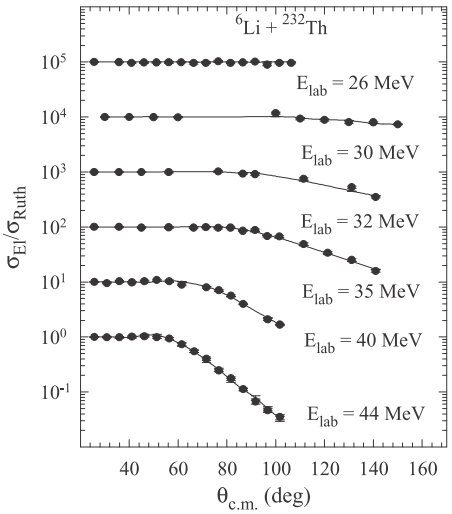

FIG. 3. Experimental elastic scattering cross section (σ_{El}) normalized to the Rutherford cross section (σ_{Ruth}) as a function of $\theta_{c.m.}$ for the ^{6}Li + ^{232}Th system (solid circles) (suitably scaled up for each energy) and their best fits from optical model calculations (solid lines). The curves correspond to the best fits obtained by using the ECIS code.

parts of different optical potentials that fitted the data cross each other, as shown in Fig. 4(a) and 4(b) at 44 MeV for the ^{6}Li + ^{232}Th system. For the ^{7}Li + ^{232}Th system the real sensitive radii values are observed to be in the range of 12.6 to 9.5 fm with an average of $R_{Sr} = 11.5$ fm and the imaginary sensitive radii values range from 12.7 to 8.5 fm with an average value of $R_{Si} = 11.05$ fm. A mean sensitive radius of $R_s = 11.27$ fm for the ^{7}Li + ^{232}Th system (the average between $R_{Sr} = 11.50$ fm and $R_{Si} = 11.05$ fm) was obtained to derive the energy dependence of the real and imaginary potentials. Similarly for the ^{6}Li + ^{232}Th system, the average sensitive radius was $R_s = 12.14$ fm (the average between $R_{Sr} = 12.05$ fm, and $R_{Si} = 12.23$ fm). The values of radius parameters for the real and imaginary parts were kept fixed at 1.06 fm for all the calculations for ^{6,7}Li + ^{232}Th systems in the analysis. A similar fitting procedure can also be found in the literature [8,15,16].

B. Analysis using the double-folding Sao Paulo potential

The SPP [20,21] is an optical potential that has been successfully used to describe a large variety of systems in a wide energy range, including fusion excitation functions and barrier distributions of weakly bound nuclei [25,26]. This potential is based on the Pauli nonlocality involving the exchange of nucleons between the projectile and the target. For a limited range of energy, as in the present work, it can be considered as the usual double-folding potential based on an extensive systematization of nuclear densities extracted from elastic scattering data. The imaginary part of the interaction is assumed to have the same shape as the real part, with one single adjustable parameter N_I related to its strength. The data-fit procedure is performed with only two free parameters, the normalization factors for the real and the imaginary parts,

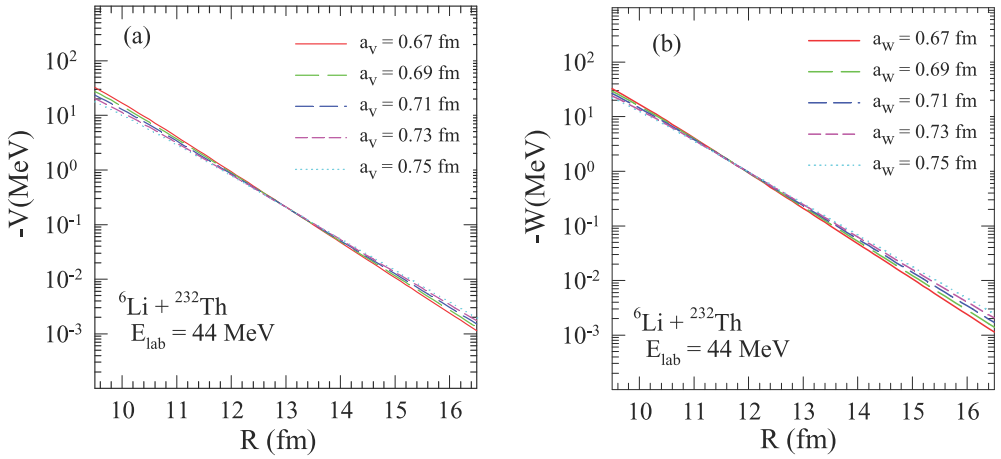

FIG. 4. (Color online) Several potentials that produce similar fits of the data, for 44 MeV. The crossing point are the derived real (a) and imaginary (b) sensitivity radii.

N_R and N_I. The energy-dependent normalization coefficients N_R and N_I take into account the effects of the dynamical polarization potential due to direct channel couplings. These dynamical polarization potentials are directly related to a dispersion relation. The present elastic scattering angular distribution analysis with the Sao Paulo potential follows the prescription given by Gomes *et al.* [10]. The curves resulting from the best fits using the SPP overlap with the calculations of the Wood-Saxon potential and therefore are not shown in Figs. 2 and 3. The resulting fits of the normalization parameters are listed in Tables I and II for ^{7}Li + ^{232}Th and ^{6}Li + ^{232}Th systems, respectively. It can be observed that the energy dependence (Fig. 6) follows the results from previous analysis similarly. So, our conclusions concerning the behavior of the optical potential energy dependence do not change when either of the potentials is used.

IV. DISPERSION RELATION ANALYSIS

An elastic scattering dispersion relation analysis has been carried out for ^{6,7}Li + ^{232}Th systems in order to qualitatively understand the experimental results on the energy dependence of the real and imaginary potentials. In the study of the dispersion relation, the optical potentials are fixed and only the depth parameters are varied so that it is valid at all radii. The dispersion relation for the optical model of elastic scattering is given as [1,2,27,28]

$$\Delta V(E) = \frac{P}{\pi} \int_{-\infty}^{+\infty} \frac{W(E')}{E' - E}\, dE', \qquad (1)$$

where P denotes the principal value. Equation (1) allows us to evaluate ΔV, the dispersive contribution to the real part, from knowledge of empirical values of the optical model absorption term $W(E)$ at sensitive radius.

Equation (1) indicates that, at energies where the absorption increases rapidly, the real part of the potential gets more attractive (i.e., ΔV is negative) than in the regions where the absorption remains constant or changes gradually [29]. This behavior has indeed been observed at energies near the top of the Coulomb barrier, where the rapid variation in the strength of the empirical real part has been called the threshold anomaly. According to the dispersion relation formulation, this variation in $V(E)$ is related to the rapid changes occurring in the imaginary term due to the opening of reaction channels as the Coulomb barrier is surpassed. In this work, the dispersion relation has been applied as a function of E at the sensitive radius (R_s) to the phenomenological optical model potentials, determined at each energy between 24 to 44 MeV for both ^{6,7}Li + ^{232}Th systems. The linear segment model proposed in Ref. [30] was used in the imaginary part in order to get the real part. In the ^{7}Li + ^{232}Th system, three sets of the real potential $V(E)$ were obtained by numerical integration of Eq. (1) using three sets of different line segment fits of the imaginary potential $W(E)$ [29]. Similarly, the energy dependence of the real and the imaginary parts of the SPP are shown in Fig. 6. N_R is obtained by means of the dispersion relation using the same procedure as in the case of the phenomenological potential previously described. One can observe results similar to those from the WSP approach. In the past, several studies were carried out in order to observe the energy-dependent behavior of the real and imaginary parts of the optical potential in the dispersion relation calculations near and below the barrier energies [8,10–12,15–18]. However, in some recent studies [8,10], important differences in the interpretation of the dispersion relations of the two lithium isotopes around the barrier energies have arisen. Figure 5 shows the energy dependence of the potential parameters for both systems ^{6,7}Li + ^{232}Th. The solid points represent the values of the real and the imaginary potentials derived by using the sensitivity radius using the Wood Saxon optical potential. The solid and the dashed curves represent the analysis using the dispersion relation. Similarly, Fig. 6 shows the energy dependence of the normalization factors N_R and N_I, for the real and the imaginary potentials with the SPP (solid points). The solid and dashed curves indicate the behavior of N_R and N_I with the dispersion relation. In the case of the ^{7}Li + ^{232}Th system, both analyses show similar trends (Figs. 5 and 6). It can be clearly seen that the real potential first increases and then decreases below the barrier, while the imaginary part of the potential decreases below the barrier. This behavior is

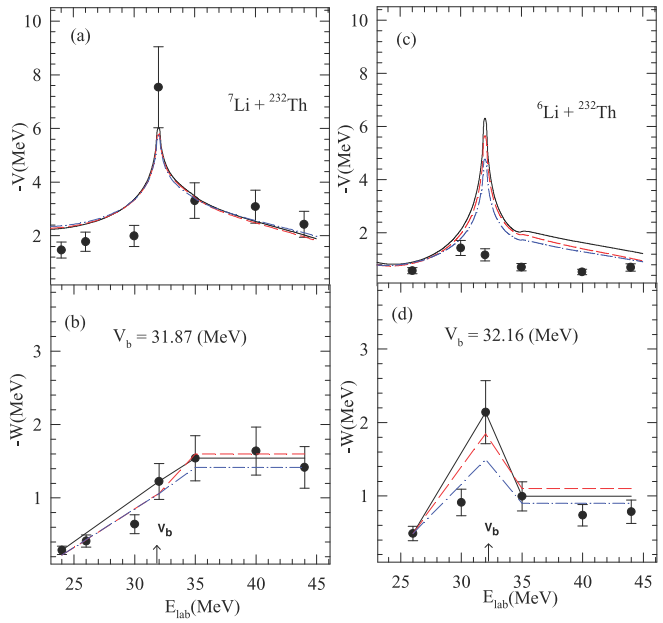

FIG. 5. (Color online) Energy dependence of the real and imaginary potentials at $R_s = 12.14$ fm and 11.27 fm for ^{6}Li + ^{232}Th and ^{7}Li + ^{232}Th systems, respectively. The straight line segments represent various fits of imaginary potential $W(E)$; the corresponding curves for real potential $V(E)$ were obtained from these by using the dispersion relation. Panels (a) and (b) correspond to the real and imaginary potential curves for the ^{7}Li + ^{232}Th system, whereas (c) and (d) represent the ^{6}Li + ^{232}Th system.

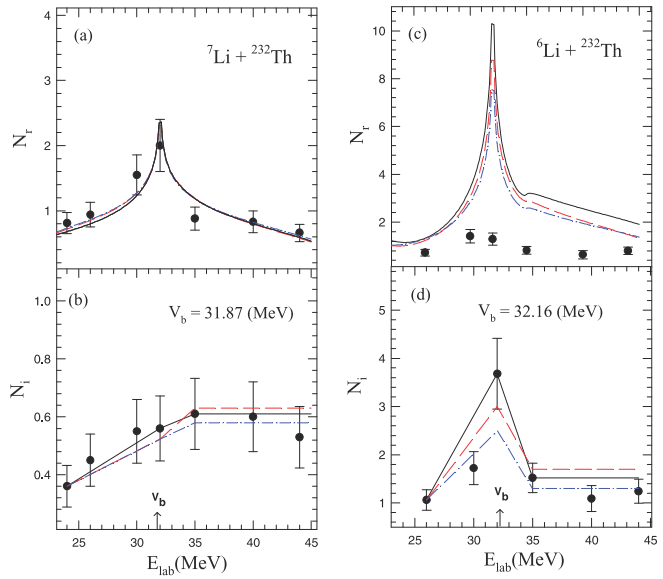

FIG. 6. (Color online) Energy dependence of the normalization factors N_R and N_I, for the real and imaginary potentials, corresponding to the Sao Paulo potential with two free parameters, for the ^{6}Li + ^{232}Th and ^{7}Li + ^{232}Th systems. The lines represent possible behaviors of N_R and N_I that are compatible with the dispersion relation [2,10]. Panels (a) and (b) correspond to the real and imaginary potential curves for the ^{7}Li + ^{232}Th system, whereas (c) and (d) represent the ^{6}Li + ^{232}Th system.

supported by the analysis of the dispersion relation that fits the data appreciably well. Thus it may be concluded that elastic scattering of the ^{7}Li + ^{232}Th system has the usual threshold anomaly, as indicated by a characteristic localized peak in the real part and a corresponding decrease of the imaginary part of the potential as the bombarding energy decreases toward the Coulomb barrier. The present inferences are in agreement with that reported by others in the literature [8,16,31].

For the ^{6}Li + ^{232}Th system, the imaginary part of the potential shows an increase, although limited to one point only, and then it decreases as the bombarding energy decreases toward the Coulomb barrier. On the other hand, the real part of the optical potential slightly increases and then shows a decreasing trend below the barrier energy. This trend is definitely in contrast to what has been observed in the case of the ^{7}Li + ^{232}Th system. This is an indication of the absence of a normal TA in the ^{6}Li + ^{232}Th system. This is obvious because, in the reactions with the ^{6}Li projectile, breakup is

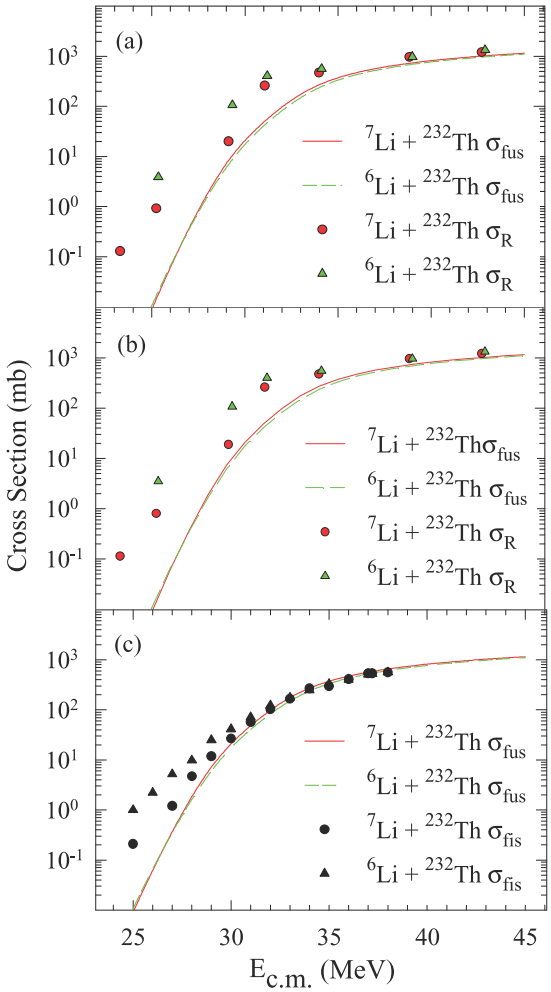

FIG. 7. (Color online) The total fusion cross sections (σ_{fus}) calculated by CCFULL and total reaction cross sections (σ_R) for the ^{6,7}Li + ^{232}Th systems obtained by using (a) the ECIS code and (b) the SPP calculation, plotted as a function of the bombarding energy. The total fission cross sections (σ_{fis}) [33] and the total fusion cross sections for the ^{6,7}Li + ^{232}Th systems are plotted in (c).

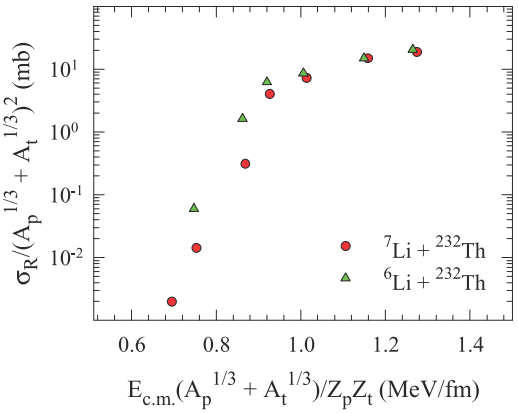

FIG. 8. (Color online) Reduced total reaction cross section vs reduced projectile energy for the ^{6,7}Li + ^{232}Th reactions using the prescription given in Ref. [40].

the dominant channel, unlike in the case of the ^{7}Li projectile where the breakup channel is far above its first excited state. Similar results for the TA and the BTA have also been reported for ^{6,7}Li + ^{80}Se systems [7]. This indicates that the ^{6}Li + ^{232}Th system shows the presence of a BTA, whereas the ^{7}Li + ^{232}Th system shows a normal TA.

V. TOTAL REACTION CROSS SECTION

The fusion cross sections have been calculated for ^{6,7}Li + ^{232}Th systems by using the CCFULL code [32]. The energy range used in the calculation was 24 to 44 MeV, in steps of 1 MeV. In the present work, the total reaction cross sections derived from the experimental elastic scattering data for ^{6,7}Li + ^{232}Th systems were compared with the calculated fusion cross sections and measured fission cross section values taken from the literature [33] as shown in Figs. 7(a), 7(b), and 7(c). The total reaction cross sections obtained from the optical model ECIS code and the SPP calculation have larger values for the ^{6}Li + ^{232}Th system in comparison to the ^{7}Li + ^{232}Th system, for all energies as shown in Fig. 7. The reaction cross sections are predominantly enhanced compared to CCFULL calculations at sub-barrier energies. From Fig. 7, it is also seen that the fission cross section has a strong enhancement for the ^{6}Li projectile at sub-barrier energies. At above-barrier energies the fusion-fission process is dominant, but at lower energies the breakup fusion-fission process becomes important and hence the fission cross section for the ^{6}Li + ^{232}Th system is enhanced at sub-barrier energies. This may be an indication that the inclusive breakup reaction cross section is significantly more for ^{6}Li compared to the ^{7}Li projectile. These results are similar to the earlier measurements of ^{6}Li on ^{28}Si and ^{208}Pb [34,35], where the yield of α particles indicates the breakup contribution in ^{6}Li. However, more coincidence measurements with the reaction products will provide a better understanding of the enhanced breakup probability for ^{6}Li. The role of projectile structure in the reaction dynamics and the influence of the breakup process in the fusion cross sections at energies near the Coulomb barrier have also been reported earlier for weakly as well as tightly bound projectiles [36–39]. In order to eliminate the projectile size effects on the reaction cross sections for ^{6,7}Li + ^{232}Th systems, the "reduction" method was used. This method was proposed by Gomes *et al.* [40] and has been well implemented by others [16,41,42]. The reduced cross section values were calculated at all energies for both systems. In this method, the quantities $\sigma_R/(A_P^{1/3} + A_T^{1/3})^2$ versus $E_{c.m.}\,(A_P^{1/3} + A_T^{1/3})/Z_P Z_T$ are plotted, where P and T represent the projectile and the target, respectively, and σ_R is the total reaction cross section. As shown in Fig. 8, it can be seen that the total reduced reaction cross section for ^{6}Li is larger than that for ^{7}Li, below the barrier. This is again an indication of higher breakup probability in the case of ^{6}Li and is also in agreement with the earlier observations [7,16,29].

VI. SUMMARY AND CONCLUSIONS

Elastic scattering angular distribution measurements have been carried out for the ^{6,7}Li + ^{232}Th systems at several bombarding energies from below to well above the Coulomb barrier. The experimental data have been analyzed by using the WSP and SPP double-folding forms of phenomenological optical potentials. The relevant parameters that give a best fit to the elastic scattering angular distribution were obtained through a χ^2-minimization procedure. The behavior of the corresponding parts of the potential as a function of energy is consistent with a situation close to the threshold anomaly for the ^{7}Li + ^{232}Th system. The increasing trend around the barrier of the imaginary part of the phenomenological potential as a function of energy indicates the absence of the usual threshold anomaly for the ^{6}Li + ^{232}Th system and this may be interpreted as evidence of the breakup threshold anomaly. The enhanced reaction cross sections have been observed at sub-barrier energies for the ^{6}Li + ^{232}Th system in comparison to the ^{7}Li + ^{232}Th system. It will be interesting to have more exclusive measurements in order to understand the higher breakup probabilities for the ^{6}Li projectile.

ACKNOWLEDGMENTS

We thank the operating staff of the BARC-TIFR Pelletron, Mumbai, India, for the smooth running of the machine during the experiment. SD and SM acknowledge UGC-DAE-CSR, Kolkata, for financial support through a major research project.

[1] M. A. Nagarajan, C. C. Mahaux, and G. R. Satchler, Phys. Rev. Lett. **54**, 1136 (1985).
[2] G. R. Satchler, Phys. Rep. **199**, 147 (1991).
[3] M. E. Brandan and G. R. Satchler, Phys. Rep. **285**, 143 (1997).
[4] P. Singh, S. Kailas, A. Chatterjee, S. S. Kerekatte, A. Navin, A. Nijasure, and B. John, Nucl. Phys. A **555**, 606 (1993).
[5] J. Lubian *et al.*, Nucl. Phys. A **791**, 24 (2007).
[6] F. A. Souza *et al.*, Phys. Rev. C **75**, 044601 (2007).
[7] L. Fimiani *et al.*, Phys. Rev. C **86**, 044607 (2012).
[8] A. M. M. Maciel *et al.*, Phys. Rev. C **59**, 2103 (1999).
[9] N. Keeley, S. J. Bennett, N. M. Clarke, B. R. Fulton, G. Tungate, P. V. Drumm, M. A. Nagarajan, and J. S. Lilley, Nucl. Phys. A **571**, 326 (1994).
[10] P. R. S. Gomes *et al.*, J. Phys. G **31**, S1669 (2005).

[11] M. S. Hussein, P. R. S. Gomes, J. Lubian, and L. C. Chamon, Phys. Rev. C **73**, 044610 (2006).
[12] J. M. Figueira *et al.*, Phys. Rev. C **75**, 017602 (2007).
[13] M. Biswas *et al.*, Nucl. Phys. A **802**, 67 (2008).
[14] M. Zadro *et al.*, Phys. Rev. C **80**, 064610 (2009).
[15] H. Kumawat *et al.*, Phys. Rev. C **78**, 044617 (2008).
[16] N. N. Deshmukh *et al.*, Phys. Rev. C **83**, 024607 (2011).
[17] J. M. Figueira *et al.*, Phys. Rev. C **81**, 024613 (2010).
[18] S. Santra, S. Kailas, K. Ramachandran, V. V. Parkar, V. Jha, B. J. Roy, and P. Shukla, Phys. Rev. C **83**, 034616 (2011).
[19] A. Gomez Camacho, P. R. S. Gomes, and J. Lubian, Phys. Rev. C **82**, 067601 (2010).
[20] L. C. Chamon, D. Pereira, M. S. Hussein, M. A. Candido Ribeiro, and D. Galetti, Phys. Rev. Lett. **79**, 5218 (1997).
[21] L. C. Chamon *et al.*, Phys. Rev. C **66**, 014610 (2002).
[22] J. Raynal, Phys. Rev. C **23**, 2571 (1981).
[23] D. Patel *et al.*, Pramana-J. Phys. **81**, 587 (2013).
[24] G. R. Satchler, in *Proceedings of the International Conference on Reactions between Complex Nuclei, Nashville, TN*, edited by R. L. Robinson, F. K. McGowan, J. B. Ball, and J. H. Hamilton (North Holland, Amsterdam, 1974), Vol. 2, p. 171.
[25] E. Crema, L. C. Chamon, and P. R. S. Gomes, Phys. Rev. C **72**, 034610 (2005).
[26] E. Crema, P. R. S. Gomes, and L. C. Chamon, Phys. Rev. C **75**, 037601 (2007).
[27] B. R. Fulton, D. W. Banes, J. S. Lilley, M. A. Nagarajan, and I. J. Thompson, Phys. Lett. B. **162**, 55 (1985).
[28] A. Baeza, B. Bilwes, R. Bilwes, J. Diaz, and J. L. Ferrero, Nucl. Phys. A **419**, 412 (1984).
[29] M. M. Gonzlez and M. E. Brandan, Nucl. Phys. A **693**, 603 (2001).
[30] C. Mahaux, H. Ngo, and G. R. Satchler, Nucl. Phys. A **449**, 354 (1986).
[31] N. Keeley and K. Rusek, Phys. Rev. C **56**, 3421 (1997).
[32] K. Hagino *et al.*, Comput. Phys. **123**, 143 (1999).
[33] H. Freiesleben, G. T. Rizzo, and J. R. Huizenga, Phys. Rev. C **12**, 42 (1975).
[34] A. Pakou *et al.*, Phys. Rev. Lett. B **633**, 691 (2006).
[35] C. Signorini *et al.*, Phys. Rev. C **67**, 044607 (2003).
[36] M. Dasgupta *et al.*, Nucl. Phys. A **834**, 147c (2010).
[37] M. Dasgupta *et al.*, Phys. Rev. Lett. **82**, 1395 (1999).
[38] D. C. Biswas, R. K. Choudhury, D. M. Nadkarni, and V. S. Ramamurthy, Phys. Rev. C **52**, 2827 (1995).
[39] D. C. Biswas, R. K. Choudhury, B. K. Nayak, D. M. Nadkarni, and V. S. Ramamurthy, Phys. Rev. C **56**, 1926 (1997).
[40] P. R. S. Gomes, J. Lubian, I. Padron, and R. M. Anjos, Phys. Rev. C **71**, 017601 (2005).
[41] N. N. Deshmukh *et al.*, Eur. Phys. J. A **47**, 118 (2011).
[42] S. Mukherjee *et al.*, Eur. Phys. J. A **45**, 23 (2010).

EPJ Web of Conferences **86**, 00008 (2015)
DOI: 10.1051/epjconf/20158600008

Energy dependence of optical potential in the near barrier elastic scattering of ^{11}B from ^{232}Th

Shradha Dubey[1,2], S. Mukherjee[1], D. Patel[1], Y. K. Gupta[2], L. S. Danu[2], B. N. Joshi[2], G. K. Prajapati[2], S. Mukhopadhyay[2], B. V. John[2], B. K. Nayak[2], and D. C. Biswas[2,a]

[1] *Physics Department, Faculty of Science, M.S.University of Baroda, Vadodara-390002, India*
[2] *Nuclear Physics Division, Bhabha Atomic Research Centre, Mumbai - 400085*

Abstract. The elastic scattering cross sections of ^{11}B projectile on the ^{232}Th target have been measured at different bombarding energies close to the Coulomb barrier. The data has been analyzed for this system using the optical model ECIS code with phenomenological Woods-Saxon forms of the optical potentials. The energy dependence of the volume type real and imaginary parts of the optical potentials are derived from the best fit of the experimental angular distribution data. The total reaction cross sections are obtained from optical model analysis.

1 Introduction

The rich interplay between the intrinsic structure and the reaction dynamics of the interacting nuclei has been a hall-mark of near-barrier heavy-ion interactions [1]. One of the manifestations of this feature is a strong energy dependence of the optical model potential deduced from analyses of elastic scattering angular distributions at energies around the Coulomb barrier [1, 2]. The study of elastic scattering angular distributions determine parameters of the real and imaginary parts of the nuclear interaction potential. From systematic analysis of elastic scattering measurements involving tightly bound nuclei, the so called "threshold anomaly" (TA) has been observed in a number of systems [1]. This has been understood in terms of couplings of elastic channel to the direct reaction channels that generate an additional attractive real dynamic polarization potential. The study of the TA is important to investigate the influence of the breakup and other reaction mechanisms on the elastic and fusion channels [3–5].

In the present work, the elastic scattering angular distribution measurements have been carried out for ^{11}B + ^{232}Th system at energies from 4% below the Coulomb barrier (V_{lab} ~ 54 MeV) to approximately 20% above the barrier. The total reaction cross sections for this system have also been derived to understand the role of projectile breakup on the total reaction cross sections. The present article has been organized in the following way. The experimental set up is described in Sec.2. Data analysis using the Wood-Saxon potential (WSP) to determine the energy dependence of potential parameters have been discussed in Sec.3. In Sec.4, a systematic study of total reaction cross section for ^{11}B + ^{232}Th system has been discussed. In Sec.5, the summary and conclusions of the present work are reported.

2 Experimental procedure

The experiment was performed at the 14UD BARC-TIFR Pelletron facility at Mumbai using beams of ^{11}B in a wide energy range around the Coulomb barrier, i.e., 52, 53, 54, 55, 56, 57, 59, 61 and 65 MeV for ^{11}B + ^{232}Th system. The observed uncertainty in the beam energy was about 1% for all the selected energies. A self supporting ^{232}Th target of thickness 1.5 mg/cm^2 was placed at the center of the general purpose scattering chamber and the elastically scattered ^{11}B particles were detected by silicon ΔE-E telescopes mounted on a movable arm of the chamber. Four telescopes of thickness (T_1) with ΔE = 25 μm and E = 300μm, (T_2) with ΔE = 40 μm and E = 300 μm, (T_3) with ΔE = 25 μm and E = 300 μm and (T_4) with ΔE = 25 μm and E = 300 μm were used in the experiment. The detector telescopes were placed at an angular separation of 10° and two silicon detectors with thickness around 300 μm were mounted at fixed angles ±18° with respect to beam direction for absolute normalization and beam monitoring. The angular distributions were measured in steps of 5° in the angular range from 35° to 170°. The uncertainty on the angular range of each telescope was ±0.81°.

3 Optical Model Analysis Of Elastic Scattering

The optical model fits to the elastic scattering data have been performed using the ECIS code [6]. The phe-

[a] corresponding author:dcbiswas@barc.gov.in

nomenological Woods-Saxon form of the interaction potential with only volume terms have been used in the analysis. To obtain the starting parameters, a global best fit procedure for all energies were performed, using the three parameters characterized by real and imaginary depth of the potential, reduced radii (r_o) and diffuseness (a_v and a_w). Thereafter, in order to avoid a fit procedure with too many parameters, the real and imaginary reduced radii were fixed at 1.06 fm for the ^{11}B + ^{232}Th system, similar to the value used earlier [4, 5]. Using this radius, and varying the diffuseness parameters a_v and a_w (real and imaginary respectively) within the interval from 0.67 fm to 0.75 fm, an attempt was made to obtain the best possible parameters of the optical potential that best describe the elastic scattering angular distribution. In the present work, the best possible fitted values were obtained for a_v, a_w = 0.71 fm. The real and imaginary radius parameters (r_o = 1.06 fm) and diffuseness parameters (a_v, a_w = 0.71 fm) were fixed for all energies. The depths of real and imaginary potentials were varied to obtain minimum value of χ^2 for the ^{11}B + ^{232}Th system.

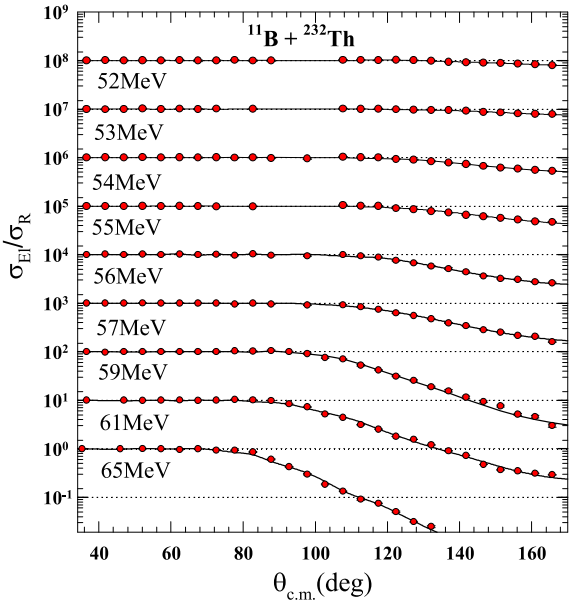

Figure 1. Experimental elastic scattering cross section normalized to the Rutherford cross section as a function of $\theta_{c.m.}$ for ^{11}B + ^{232}Th system.

Table 1. Optical model parameters obtained by fitting the experimental elastic differential cross section data using the ECIS code for ^{11}B + ^{232}Th system.

E_{lab}(MeV)	V_r(MeV)	V_i(MeV)	$\frac{\chi^2}{n}$	$\sigma_R(mb)$
52	194.0	0.131	1.582	7.02
53	149.2	15.03	0.640	29.81
54	162.0	31.43	1.210	89.74
55	134.2	27.32	4.060	105.4
56	126.0	51.44	3.523	216.2
57	109.4	57.02	4.700	279.7
59	121.5	59.23	4.900	432.6
61	73.67	89.30	11.21	601.7
65	53.45	109.7	9.210	886.4

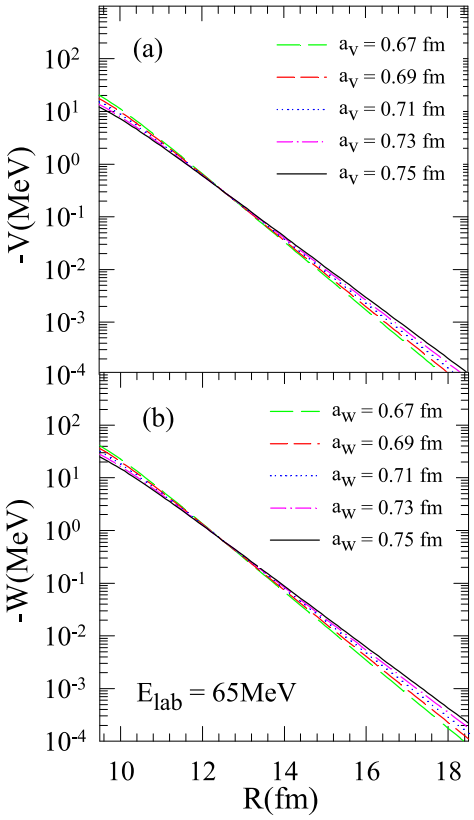

Figure 2. Several potential that produce similar fits of the data, for 65 MeV. The crossing point are the derived real (a) and imaginary (b) sensitivity radii for ^{11}B + ^{232}Th system.

The potential parameter values for the best fit and the total reaction cross sections are shown in Table-I. The best fit optical model parameters show significant energy dependence as reflected from Table-I, which is a characteristic feature of the elastic scattering. The solid lines in Fig. 1 show the best fit of the experimental data for the elastic scattering angular distributions for ^{11}B + ^{232}Th system.

To reduce the ambiguities of the best fitted parameters of the optical potential, the strong sensitive radius R_{Sr} and R_{Si} corresponding to the real and imaginary potential were determined. For this purpose the radius parameters were kept fixed and the depth parameters of the real and imaginary potentials were fitted by varying the diffuseness from 0.67 to 0.75 fm, in step of 0.02 fm for all energies of ^{11}B + ^{232}Th system. The strong sensitive radii [8] were determined, where the real and imaginary part of different optical potentials that fitted the data cross each other as shown in Fig. 2 (a) and 2(b) for 65 MeV for ^{11}B + ^{232}Th system. The real sensitive radii values were observed to be in the range of 12.4 to 11.3 fm with a average of R_{Sr} = 11.57 fm and for the imaginary sensitive radii values range from 12.7 to 13.5 fm with a average value of R_{Si} = 13.34 fm. A mean sensitive radius of R_s = 12.45 fm for ^{11}B + ^{232}Th system (average between R_{Sr} = 11.57 fm and R_{Si}

= 13.34 fm) was obtained to derive energy dependence of real and imaginary potential. In the analysis for this system the values of radius parameters for real and imaginary parts were kept fixed at 1.06 fm for all the calculations. A similar fitting procedure can also be found in the literature [2, 7] for ^{11}B + ^{209}Bi system. The corresponding values of the energy dependence of the real and imaginary potentials for the ^{11}B + ^{232}Th system are shown in Fig. 3. The error bars in Fig. 3 represent the range of deviation of the potential corresponding to a χ^2 variation of one unit.

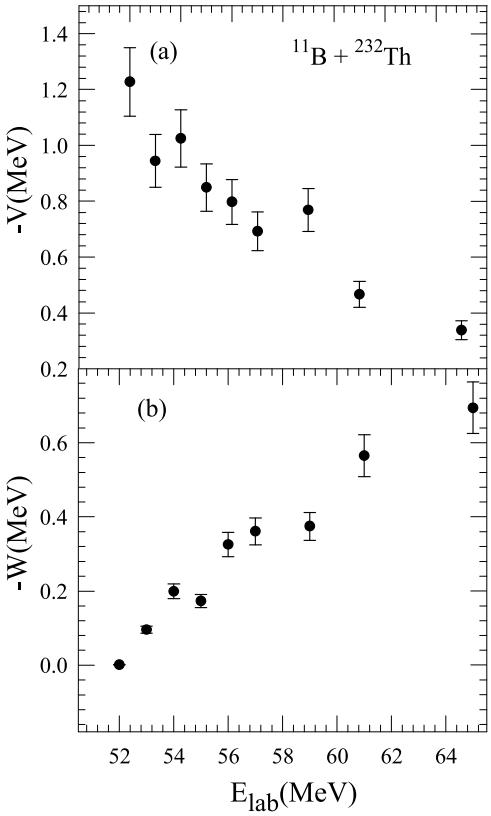

Figure 3. Energy dependence of the real and imaginary parts of the optical potential obtained for the ^{11}B + ^{232}Th system at an average radius R_s = 12.45 fm.

4 Total Reaction Cross Section

The fusion cross sections have been calculated for ^{11}B + ^{232}Th system by using CCFULL code [9]. The energy range used in the calculation was 52 to 65 MeV, in steps of 1 MeV. In the present work, the total reaction cross sections derived from experimental elastic scattering data analysis for ^{11}B + ^{232}Th system was compared with the calculated fusion cross sections as shown in Fig. 4 (a). The total reaction cross sections obtained from optical model ECIS code. In order to eliminate the projectile size effect on the reaction cross sections for ^{11}B + ^{232}Th system, the "reduction" method was used. This method was proposed by Gomes et al. [10] and has been well implemented by others [4, 5, 11, 12]. The reduced cross section values were calculated at all energies for the system. In this

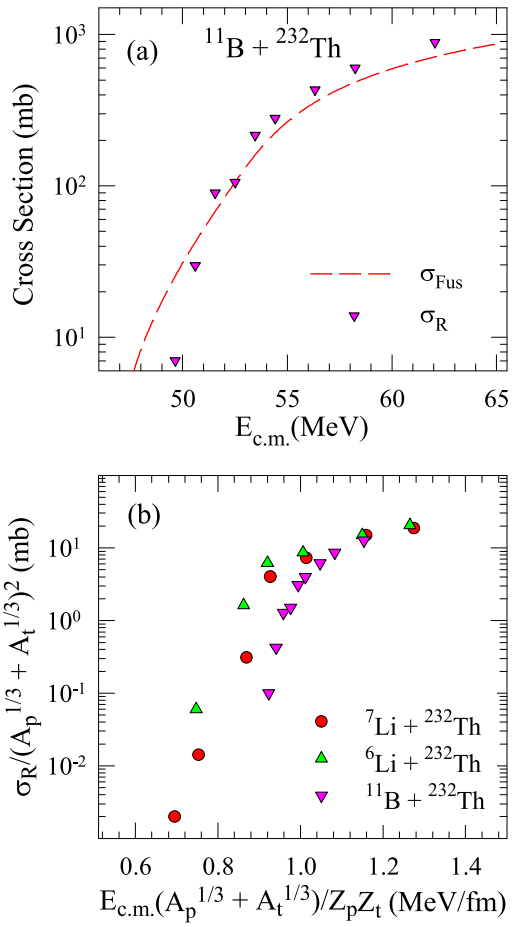

Figure 4. Total fusion cross section (σ_{fus}) (by CCFULL) and total reaction cross section (σ_R) for ^{11}B + ^{232}Th system as a function of the bombarding energy in 4 (a). Reduced total reaction cross section vs reduced projectile energy for the ^{6,7}Li + ^{232}Th and ^{11}B + ^{232}Th reactions using the prescription given in Ref. [10] in 4 (b).

method, the quantities $\sigma_R/\ (A_P^{1/3} + A_T^{1/3})^2$ vs $E_{c.m.}$ $(A_P^{1/3} + A_T^{1/3})/Z_PZ_T$ are plotted, where P and T represent the projectile and target respectively, and σ_R is the total reaction cross section. As shown in Fig. 4 (b), it can be seen that total reduced reaction cross section of ^{11}B + ^{232}Th system is smaller than ^{6,7}Li + ^{232}Th system.

5 Summary and Conclusions

The elastic-scattering angular distribution measurements have been carried out for the ^{11}B + ^{232}Th system at several bombarding energies from below to well above the Coulomb barrier. The experimental data have been analyzed using the ECIS code forms of phenomenological optical potentials. The relevant parameters that gives best fit to the elastic scattering angular distribution, were obtained through a χ^2-minimization procedure. The enhanced reaction cross sections have been observed at sub-barrier energies for ^{6,7}Li + ^{232}Th systems [5] in comparison to the ^{11}B + ^{232}Th system. This may be an indication that ^{11}B has a lower breakup probability as compared to ^{6,7}Li projectiles.

Acknowledgement

We are thankful to the operating staff of the BARC-TIFR pelletron, Mumbai, India, for smooth running of the machine during experiment. The authors S.D. and S.M. thank the UGC-DAE-CSR, Kolkata for financial support through a major research project.

References

[1] G. R. Satchler, Phys. Rep. **199**, 147 (1991).
[2] A. Shrivastava, S. Kailas, P. Singh, A. Chatterjee, A. Navin, A. M. Samant, V. Ramdev Raj, S. Mandal, S. K. Datta, S. K. Datta, Nucl. Phys. A **635**, 411 (1998).
[3] J. Lubian *et al.*, Nucl. Phys. A **791**, 24 (2007).
[4] N. N. Deshmukh *et al.*, Phys. Rev. C **83**, 024607 (2011).
[5] Shradha Dubey *et al.*, Phys. Rev. C **89**, 014610 (2014).
[6] J. Raynal, Phys. Rev. C **23**, 2571 (1981).
[7] S. Y. Lee and W. Y. So, Eur. Phys. J. A **791**, 24 (2007).
[8] G. R. Satchler, in Proceeding of the International Confrence on reactions between complex Nuclei, Nashville,TN, edited by R. L.Robinson, F. K. McGowan, J. B. Ball and J. H. Hamilton(North Holland, Amsterdam, 1974, vol. 2, P. 171.
[9] K. Hagino *et al.*, comput. Phys. commun. **123**, 143 (1999).
[10] P. R. Gomes, J. Lubian, I. Padron, R. M. Anjos, Phys. Rev. C **71**, 017601 (2005).
[11] N. N. Deshmukh *et al.*, Eur. Phys. J. A **47**, 118 (2011).
[12] S. Mukherjee *et al.*, Eur. Phys. J. A **45**, 23 (2010).

Quasi-elastic scattering and transfer angular distribution for ^{10,11}B + ^{232}Th systems at near-barrier energies

Shradha Dubey,[1,2,*] D. C. Biswas,[1,†] S. Mukherjee,[2] D. Patel,[2,‡] Y. K. Gupta,[1] G. K. Prajapati,[1] B. N. Joshi,[1] L. S. Danu,[1] S. Mukhopadhyay,[1] B. V. John,[1] S. V. Suryanarayana,[1] and R. P. Vind[1]

[1]*Nuclear Physics Division, Bhabha Atomic Research Centre, Mumbai 400085, India*

[2]*Physics Department, Faculty of Science, M.S. University of Baroda, Vadodara 390002, India*

(Received 31 March 2016; revised manuscript received 16 September 2016; published 14 December 2016)

Quasi-elastic scattering and transfer angular distributions for ^{10,11}B + ^{232}Th reactions have been measured simultaneously in a wide range of bombarding energies around the Coulomb barrier. The quasi-elastic angular distribution data are analyzed using the optical model code ECIS with phenomenological Woods-Saxon potentials. The obtained potential parameters suggest the presence of usual threshold anomaly, confirming tightly bound characteristics for both the projectiles. The reaction cross sections are obtained from the fitting of quasi-elastic angular distribution data. The reduced cross sections at sub-barrier energies compared with ^{6,7}Li + ^{232}Th systems show a systematic dependence on projectile breakup energy. The angular distribution of the transfer products show similar behavior for both the systems.

DOI: 10.1103/PhysRevC.94.064610

I. INTRODUCTION

In heavy ion reactions, the interplay between the intrinsic structure and the reaction dynamics of the interacting nuclei is very important at energies near the Coulomb barrier. The study of elastic scattering and transfer processes in these reactions provides rich information on various reaction channel couplings. Several aspects of heavy ion reactions have been investigated over recent decades from the analysis of elastic scattering data using different optical model codes. One of the most important features of the heavy ion elastic scattering at energies close to the Coulomb barrier is the peculiar behavior of the optical potential, known as the threshold anomaly (TA) [1]. The real and imaginary optical potential parameters vary strongly at beam energies below the Coulomb barrier. The rapid decrease of the imaginary part of the optical potential below the barrier leads to a local peak in real part and this behavior can be understood using a dispersion relation between the real and the imaginary parts of the optical potential [1–4]:

$$\Delta V(E) = \frac{P}{\pi} \int_{-\infty}^{+\infty} \frac{W(E')}{E' - E}\, dE'. \tag{1}$$

Also,

$$V(E) = V_o + \Delta V(E), \tag{2}$$

where P is the principal value of the integral, $V(E)$ is dynamical real potential, and ΔV is dynamical polarization potential. Here, V_o is independent of energy and $W(E)$ is the energy-dependent imaginary potential.

The threshold anomaly phenomena have been studied extensively in heavy ion reactions involving either weakly or tightly bound projectiles [4–15]. For weakly bound projectiles, breakup threshold anomaly (BTA) has been observed, where a repulsive polarization potential is generated due to the coupling of breakup channels to the elastic scattering, which causes an increase in the imaginary potential and corresponding decrease in the real part [16–18]. We have reported earlier the presence of BTA in the case of the ^{6}Li + ^{232}Th system. Although the breakup threshold for ^{7}Li (2.47 MeV) is not significantly larger than ^{6}Li (1.48 Mev), still ^{7}Li + ^{232}Th shows usual TA [19]. For the ^{9}Be projectile, the breakup threshold energy is 1.57 MeV and therefore it is expected to exhibit BTA. However, recently Camacho *et al.* have carried out a detailed analysis of the energy dependence of the optical potentials for the ^{9}Be + ^{208}Pb , ^{209}Bi systems [20]. It is reported that the fusion imaginary potential indicates the presence of usual TA in these reactions, similar to that observed in tightly bound systems, but the direct reaction imaginary potential shows a BTA behavior.

There are very limited elastic scattering data for ^{10}B and ^{11}B projectiles with heavy targets [14,15] and so far there have been no measurements reported for ^{10,11}B + ^{232}Th systems. The systematic investigation of the energy dependence of real and imaginary potentials for the ^{10,11}B + ^{232}Th systems is important to establish the presence of TA or BTA in these reactions. The use of the heavy target in the investigation of TA or BTA gives an advantage, as the effect is expected to be more pronounced due to large Coulomb effects. However, due to the presence of the low-lying excited states of the heavy targets, it is very difficult to separate the inelastic contributions from the elastic scattering data. In the past, optical model analysis have been carried out for quasi-elastic scattering data and it is reported that the inclusion of the inelastic channels with the elastic cross section have negligible effect on the extracted parameters [21,22].

Comparison of different reaction quantities measured simultaneously in heavy ion reactions provides useful information on the reaction mechanism as well as structural aspects of the interacting nuclei. Among them, transfer processes significantly dominate at sub-barrier energies and influence the fusion cross section [23–26]. Since we can derive the reaction

*Corresponding author: shradha30686@gmail.com

†Corresponding author: dcbiswas@barc.gov.in

‡Present address: IMP-CAS, Lanzhou, China.

cross section from elastic scattering angular distribution analysis, it is important to investigate simultaneously the transfer processes to understand the role of projectile structure in heavy ion reaction dynamics.

In the present work, we have measured simultaneously the quasi-elastic (elastic + low-lying inelastic) scattering and transfer angular distributions for ^{10,11}B +^{232}Th systems at energies from 10% below the Coulomb barrier ($V_b = 54.2$ MeV) to approximately 20% above the barrier to investigate the reaction mechanism. From the optical model analysis of the quasi-elastic angular distribution data, the potential parameters were determined to investigate the threshold anomaly for ^{10,11}B +^{232}Th systems. The experimental details are given in Sec. II. The energy dependence of potential parameters and the dispersion relation analysis are discussed in Sec. III. The analysis of transfer as well as reaction cross sections for ^{10,11}B +^{232}Th reactions are presented in Sec. IV. In Sec. V, a systematic study of reduced reaction cross section has been discussed. The summary and conclusions of the present work are presented in Sec. VI.

II. EXPERIMENTAL DETAILS

The quasi-elastic scattering and transfer angular distribution measurements were carried out using ^{10,11}B beams from the 14UD BARC-TIFR Pelletron facility, Mumbai, India, at energies $E_{\rm lab} = 52, 53, 54, 55, 56, 57, 59, 61$, and 65 MeV for the ^{11}B +^{232}Th system and 49, 51, 52, 53, 54, 55, 56, 57, 59, 61, and 65 MeV for the ^{10}B +^{232}Th system. The range of energies relative to the Coulomb barrier is ~0.96 to 1.20 for ^{11}B +^{232}Th system and it is ~0.90 to 1.19 for the ^{10}B +^{232}Th system. A self-supporting metallic foil of ^{232}Th with a thickness of 1.3 mg/cm^2 was used as target. Four silicon surface barrier detector telescopes with different thicknesses (T_1 with $\Delta E = 25\ \mu$m and $E = 300\ \mu$m; T_2, $\Delta E = 40\ \mu$m and $E = 300\ \mu$m; T_3, $\Delta E = 25\ \mu$m and $E = 300\ \mu$m; and T_4, $\Delta E = 25\ \mu$m and $E = 300\ \mu$m) were used to detect simultaneously the elastically scattered as well as projectile-like fragments. The detector telescopes were mounted on a movable arm at an angular separation of 10° inside a general-purpose scattering chamber. All four telescopes were mounted at a distance of 21.1 cm from the target, having a front collimator of 6 mm, which imposes an angular uncertainty of ±0.81°. Two monitor detectors with thickness of around 300 μm were mounted at 65 cm from the target with 1-mm collimator. They were kept at fixed angles of ±18° with respect to the beam direction, for absolute normalization and beam monitoring purposes. The angular distributions were measured in steps of 5° in the angular range from 35° to 170°. Figure 1 shows a typical two-dimensional scatter plot of the pulse heights of ΔE and $E_{\rm res}$ (residual energy) detectors for the ^{11}B +^{232}Th system at $E_{\rm lab} = 61$ MeV and $\theta_{\rm lab} = 90°$. The bounded region (dashed line) on $Z = 5$ are quasi-elastic events and the marked line width shown in the inset of Fig. 1 is used for the cross section calculation. As the width of the elastic peak is about 650 keV (FWHM), the low-lying excited states of ^{232}Th target (49.37 and 162.12 keV) could not be separated from the elastic peak in the present experimental technique. Thus, these inelastic contributions are included in quasi-elastic angular distribution data.

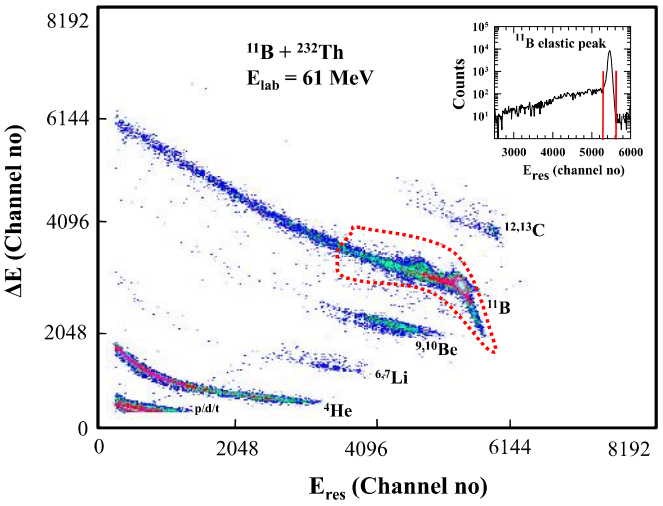

FIG. 1. A typical two-dimensional plot of ΔE versus $E_{\rm res}$ (residual energy) for the ^{11}B +^{232}Th system at $E_{\rm lab} = 61$ MeV and $\theta_{\rm lab} = 90°$. The bounded region (dashed line) on $Z = 5$ events shows quasi-elastic events and the inset in Fig. 1, shown by two vertical lines, indicates the data used for the optical model analysis.

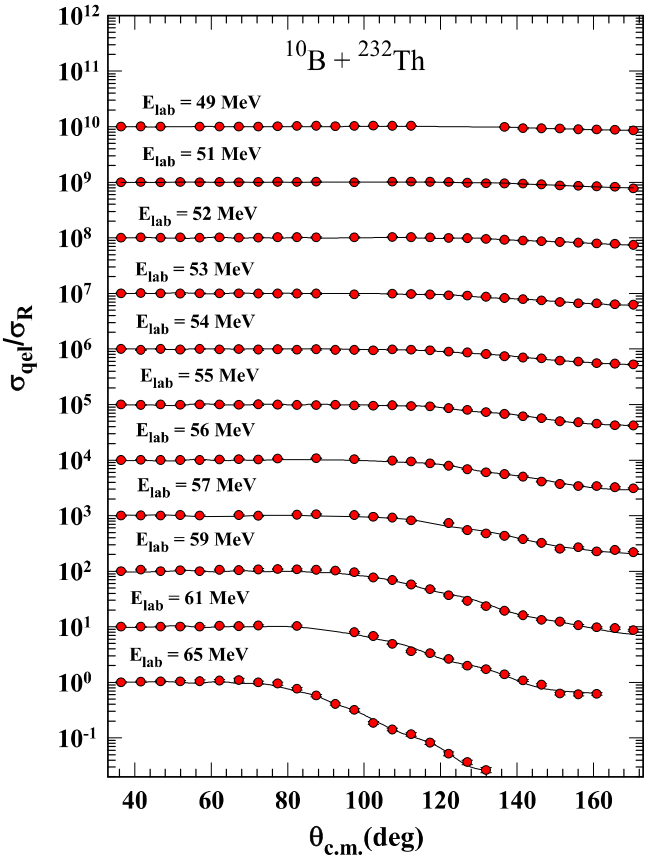

FIG. 2. Quasi-elastic ($\sigma_{\rm qel}$) scattering angular distributions normalized with Rutherford cross section ($\sigma_{\rm R}$) for the ^{10}B +^{232}Th system at various energies after suitably scaling. The solid line represents the Wood-Saxon fit (see text).

TABLE I. Optical potential parameters and reaction cross sections (σ_R) of $^{10}B + ^{232}Th$ system obtained using ECIS code. The transfer cross sections (σ_{tr}) presented here are obtained by adding the measured cross sections for $^{12,13}C$, $^{9,10}Be$, and $^{6,7}Li$.

E_{lab} (MeV)	V_r (MeV)	V_i (MeV)	$\frac{\chi^2}{n}$	σ_R (mb)	σ_{tr} (mb)
49	492.4	6.49	0.87	6.24	2.23 ± 0.47
51	294.5	11.60	0.23	16.10	4.09 ± 0.68
52	218.2	18.63	0.26	38.73	6.06 ± 1.20
53	153.0	55.74	0.21	90.97	9.64 ± 1.17
54	132.8	55.99	0.84	121.81	13.61 ± 1.42
55	128.4	50.90	0.55	153.52	16.55 ± 1.30
56	120.8	49.50	4.35	197.20	21.61 ± 1.22
57	106.4	57.23	3.48	264.91	30.18 ± 2.40
59	83.47	86.76	5.84	451.72	41.95 ± 1.66
61	59.07	84.00	3.76	551.22	48.89 ± 1.65
65	77.85	92.62	2.43	824.50	54.81 ± 4.49

III. OPTICAL MODEL ANALYSIS OF QUASI-ELASTIC SCATTERING AND DISPERSION RELATION

The experimental quasi-elastic scattering cross sections measured at several energies are plotted as a function of $\theta_{c.m}$ after normalizing with the Rutherford cross section as shown in Fig. 2. The angular distribution data are analyzed by using a phenomenological Woods-Saxon form of potential (WSP). The optical model fits to the quasi-elastic scattering data are performed using the ECIS code [27]. The WSP is an optical potential that has been successfully used in a wide range of energies to describe a large variety of reactions including inelastic scattering, fusion excitation functions, and barrier distributions. In the fitting procedure, radius parameters were initially allowed to vary with fixed depths and diffuseness parameters for both the real and imaginary parts. The analysis of the data on the entire energy range yielded a value of $r_0 = 1.06$ fm and it was kept fixed throughout in searching the other parameters. A grid search was made on the diffuseness parameters, a_v (real) and a_w (imaginary) in the range of

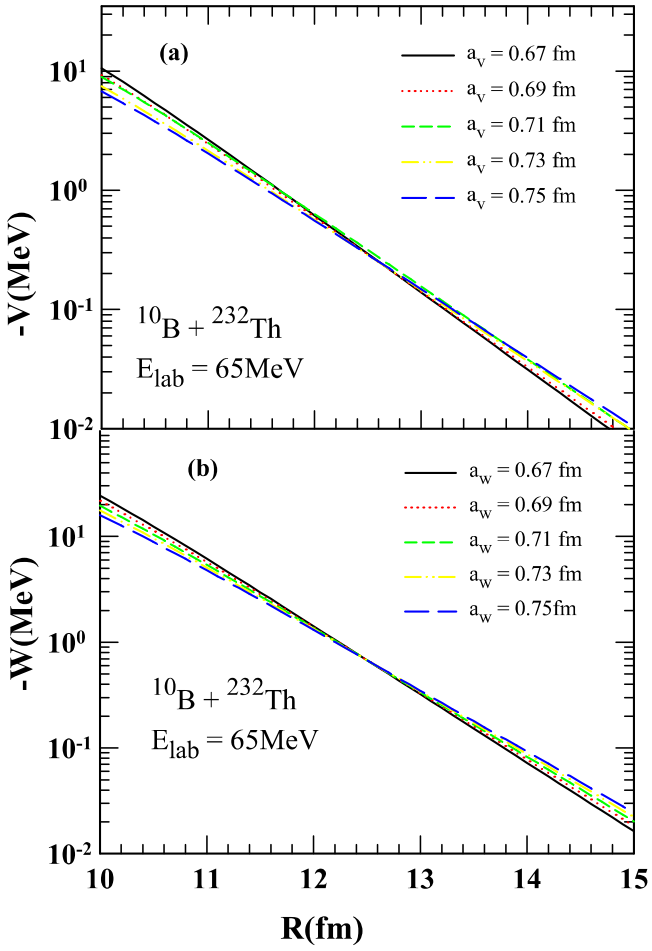

FIG. 3. Sensitivity radii based on the crossing of the real (a) and imaginary (b) parts of the WSP potential at $E_{lab} = 65$ MeV for different diffuseness parameter values (a_v and a_w).

TABLE II. Optical model parameters [28] and transfer (σ_{tr}) as well as reaction cross section (σ_R) values for the $^{11}B + ^{232}Th$ system at different energies.

E_{lab} (MeV)	V_r (MeV)	V_i (MeV)	$\frac{\chi^2}{n}$	σ_R (mb)	σ_{tr} (mb)
52	194.0	0.13	1.58	7.02	6.21 ± 0.56
53	149.2	15.03	0.64	29.81	8.39 ± 0.53
54	162.0	31.43	1.21	89.74	14.44 ± 0.93
55	134.2	27.32	4.06	105.40	16.09 ± 1.01
56	126.0	51.44	3.52	216.21	24.77 ± 1.35
57	109.4	57.02	4.70	279.72	35.75 ± 1.15
59	121.5	59.23	4.90	432.61	37.80 ± 2.16
61	73.67	89.30	11.2	601.70	38.79 ± 1.47
65	53.45	109.70	9.21	886.42	42.27 ± 1.48

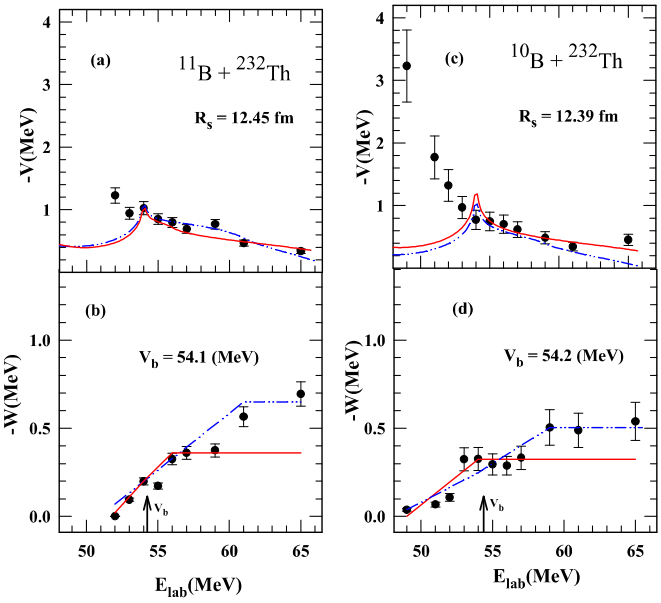

FIG. 4. Energy dependence of the real and imaginary potentials at sensitivity radii $R_s = 12.39$ fm for the $^{10}B + ^{232}Th$ system in panels (a) and (b) and at $R_s = 12.45$ fm for $^{11}B + ^{232}Th$ in panels (c) and (d). Solid (red) and dashed (blue) lines are two different sets of line-segment fits (see text). Arrows in the panels (b) and (d) indicate the positions of Coulomb barriers (V_b) for $^{11}B + ^{232}Th$ and $^{10}B + ^{232}Th$, respectively.

0.67 to 0.75 fm, in steps of 0.02 fm. For each diffuseness parameter, the potential depths, V_r (real) and V_i (imaginary), were varied to minimize χ^2. The best-fit values were obtained to be $a_v = a_w = 0.71$ fm. Thus, radius (r_0) and diffuseness parameters for both real and imaginary parts were fixed to 1.06 and 0.71 fm, respectively for all the energies. The depths of the real and imaginary potentials were varied to obtain the minimum value of χ^2. Typical best-fit calculations to the angular distributions are shown by solid lines in Fig. 2 for the ^{10}B +^{232}Th system. The best-fitted potential parameters are shown in Table I for ^{10}B +^{232}Th and in Table I ^{11}B +^{232}Th systems [28].

The angular distribution and reaction cross section values are known to be sensitive to strong absorption radius. The crossover point where depths of the potential corresponding to different diffuseness parameters intersect (see Fig. 3) is referred to as radii of sensitivity [3,8,10,11,13,29]. The radii of sensitivity R_{sr} and R_{si} corresponding to the real and imaginary parts, respectively, were determined in the present analysis. The radius parameters were kept fixed and the depth parameters of the real and imaginary parts were varied for each of the diffuseness parameters from 0.67 to 0.75 fm, in steps of 0.02 fm for all the energies. Figures 3(a) and 3(b) show typical potential families for ^{10}B +^{232}Th system at 65 MeV that give similar fits for the real and imaginary parts, respectively. At each beam energy, radii of sensitivity for both real and imaginary parts are determined. $R_{\rm sr}$ and $R_{\rm si}$ are obtained for all incident energies to be in the ranges of 11.2 to 12.4 fm and 10.9 to 15.8 fm, respectively, for the ^{10}B +^{232}Th system and in the ranges of 11.3 to 12.4 fm and 12.3 to 16.4 fm, respectively, for the ^{11}B +^{232}Th system. The average sensitive radii for the ^{10}B +^{232}Th system for full energy range are $R_{sr} = 11.67$ fm and $R_{si} = 13.12$ fm and for ^{11}B +^{232}Th system these values are $R_{sr} = 11.57$ fm and $R_{si} = 13.34$ fm. An average of R_{sr} and R_{si} was used in the dispersion relation as a effective sensitive radius R_s for both the systems. The R_s values for the ^{10}B +^{232}Th and ^{11}B +^{232}Th systems are 12.39 and 12.45 fm, respectively [28].

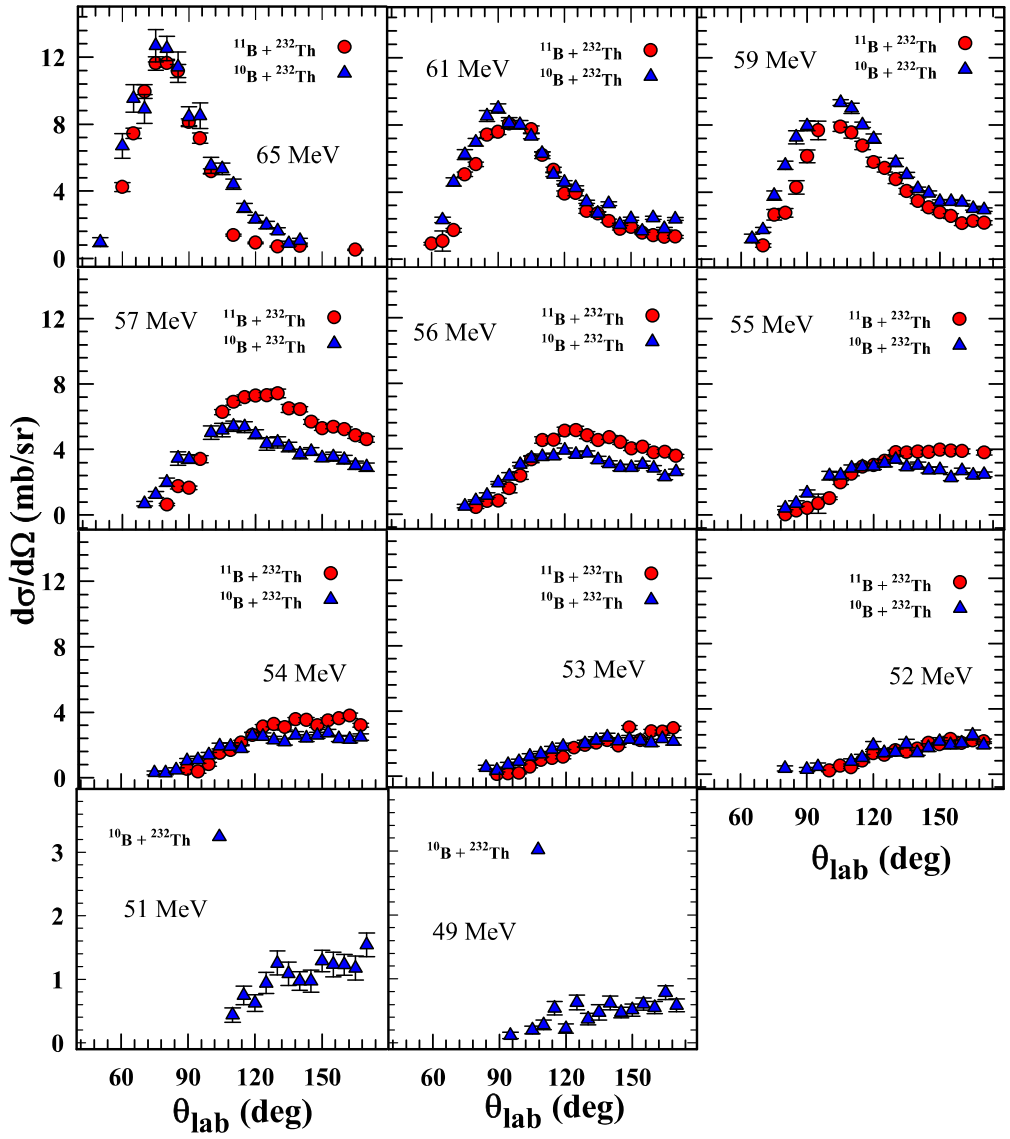

FIG. 5. Transfer angular distributions for ^{12,13}C, ^{9,10}Be, and ^{6,7}Li at various bombarding energies for ^{10,11}B +^{232}Th systems.

The energy dependence of the real and imaginary optical model potential parameters (from Tables I and II) for ^{10,11}B + ^{232}Th systems are shown in Fig. 4. The error bars in this figure represent the range of deviation of the potential corresponding to χ^2 variation of one unit. It can be observed that with the decrease in beam energy, the imaginary potential decreases and the corresponding real potential increases at energies near the Coulomb barrier. The present behaviors of real and imaginary potentials are similar to the well-known characteristics for the usual threshold anomaly, which was observed earlier for tightly bound ^{12}C, ^{16}O projectiles [4,8,11].

The dispersion relation analysis was carried out using Eq. (1) to check the consistency of the optical potentials as a function of beam energy (E). Using the knowledge of empirical values of the optical model absorption term $W(E)$ at sensitive radius (R_s), Eq. (1) allows us to evaluate ΔV, the dispersive contribution to the real part. The analysis has been performed at each energy between 52 and 65 MeV for the ^{11}B + ^{232}Th system and between 49 and 65 MeV for the ^{10}B + ^{232}Th system. In order to get the real part through the dispersion relation, the linear segment model proposed in Ref. [30] was used in the imaginary part. Two sets of the real potential $V(E)$ were obtained by numerical integration of Eq. (1) using two different line segment (red and blue lines) fits of imaginary potential $W(E)$ [31]. The dispersion relation also exhibits a local peak in real potential with rapid decrease in imaginary potential at energies below the barrier as shown in the Figs. 4(a) to 4(d). This is clearly an indication of threshold anomaly in the ^{11}B + ^{232}Th system [Figs. 4(a) and 4(b)] as well as for the ^{10}B + ^{232}Th system [Figs. 4(c) and 4(d)]. Thus, the real and imaginary optical potential parameters are consistent with the dispersion relation around the Coulomb barrier and therefore threshold anomaly is unambiguously observed in both ^{10,11}B + ^{232}Th systems. However, much below the Coulomb barrier, the dispersion relation underpredicts the experimental value of $V(E)$.

IV. ANALYSIS OF THE TRANSFER ANGULAR DISTRIBUTION

For the analysis of angular distribution of the transfer reaction products, we have measured the yield of ^{12,13}C, ^{9,10}Be, and ^{6,7}Li at various angles for both ^{10,11}B + ^{232}Th systems. The same telescopes were used for the measurement of both quasi-elastic as well as transfer products and we have normalized the data at various angles with the yield of the monitor detectors. The transfer cross sections were obtained from the yield of the transfer products at various angles comparing with the calculated Rutherford scattering cross sections at forward angles. Figure 5 shows the transfer angular distribution data for both the systems, which includes ^{12,13}C, ^{9,10}Be, and ^{6,7}Li for different bombarding energies.

In the case of ^{2}H or ^{3}H transfer from ^{10,11}B respectively, the projectile-like fragment will be ^{8}Be and it will immediately break into two α particles [32]. In the present experimental setup, only one of the α particles could be detected in the telescope. Moreover, the α particles will have contributions from compound nucleus evaporation [32]. Thus, we have not included the contribution alpha channel in the determination

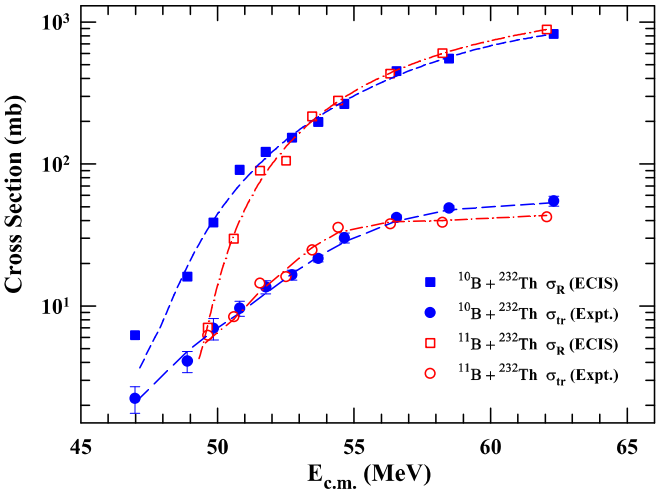

FIG. 6. Reaction cross sections for the ^{10}B + ^{232}Th system (solid square) and the ^{11}B + ^{232}Th system (open square) derived from fit to the quasi-elastic scattering angular distribution using the ECIS code. The transfer cross section (only sum of ^{12,13}C, ^{9,10}Be, and ^{6,7}Li) are plotted for ^{10}B + ^{232}Th (solid circles) and for ^{11}B + ^{232}Th (open circles). Dashed and dash-dotted lines are guides to the eye.

of the transfer cross section. The transfer data overall show a bell-shaped angular distribution at above barrier energies as shown in Fig. 5. The grazing angle corresponding to the maximum yield shifts towards back angle with the reduction of the beam energy. The angle integrated transfer cross sections were calculated from the angular distribution data for different beam energies and are listed in Tables I and II for both ^{10,11}B + ^{232}Th systems.

In the present work, we have determined the reaction cross sections for both the systems from the fitting of the quasi-elastic angular distribution data. For comparison we have plotted both the transfer and reaction cross sections in Fig. 6. It is observed that the reaction cross section values for ^{10}B + ^{232}Th reaction are significantly large in comparison to ^{11}B + ^{232}Th at sub-barrier energies. This enhancement in the cross section may be due to the contribution of the breakup-fusion process for ^{10}B + ^{232}Th reaction, because of the relatively smaller breakup threshold of the ^{10}B projectile as compared to the ^{11}B projectile.

V. UNDERSTANDING OF REDUCED REACTION CROSS SECTION

In order to study the projectile effect for different systems, it is required to suppress the differences arising from the size and the charges of the systems. A reduction methodology proposed by Gomes *et al.* has been widely used for this type of study to understand the reaction mechanism [33]. In this method, the quantities $\sigma_R/(A_P^{1/3} + A_T^{1/3})^2$ vs $E_{c.m.}(A_P^{1/3} + A_T^{1/3})/Z_P Z_T$ are plotted, where the subscripts P and T represent the projectile and target, respectively. Here, σ_R is the reaction cross section as plotted in Fig. 7(a). This analysis procedure has been successfully adopted in the past by several groups [3,19,28,29,34,35]. In the second method, the reduced reaction cross section $\sigma_R/\pi R_b^2$, is plotted as a function of the center of mass energy

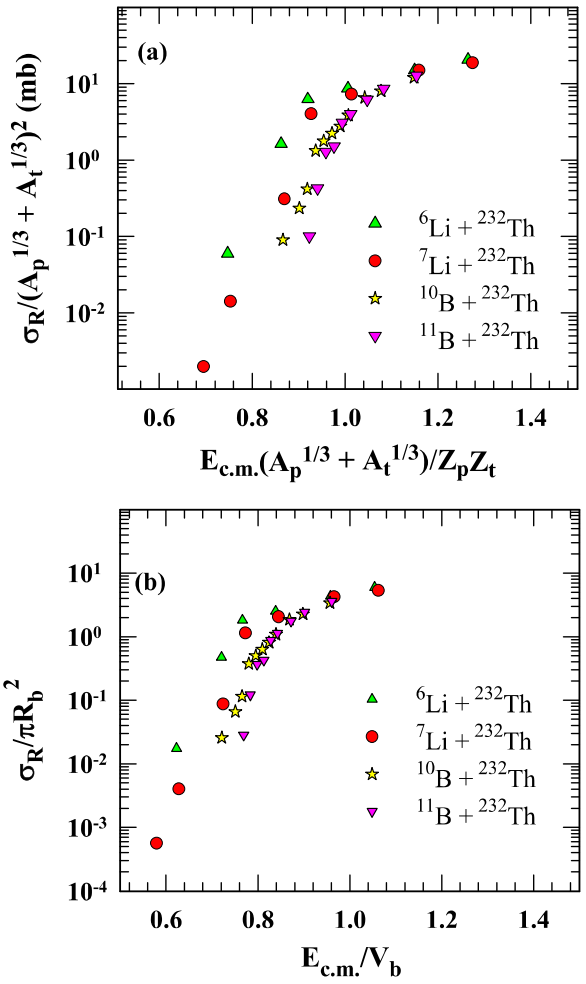

FIG. 7. Reduced reaction cross section for the ^{10,11}B + ^{232}Th systems compared with ^{6,7}Li + ^{232}Th systems [19] using the two reduction procedures (first taken from Refs. [19,33,36] and second taken from Ref. [36] as mentioned in the text).

normalized to barrier, $E_{c.m.}/V_b$ as shown in Fig. 7(b) [36]. It was suggested that the procedure removes the dependence on the charge and mass of the collision partners, but not on specific features of the projectile density, particularly when weakly bound projectile nuclei are involved. Figure 7 shows a comparison of the reduced reaction cross sections for four different projectiles (^{6,7}Li and ^{10,11}B) interacting with ^{232}Th target. It is observed that the reaction cross sections are relatively large for weakly bound ^{6}Li and ^{7}Li projectiles, because of low ^{4}He-breakup threshold energy of ^{6}Li (1.48 MeV) and ^{7}Li (2.47 MeV) as compared to ^{10,11}B (4.46 and 8.66 MeV respectively). From the systematics for all the systems, it is found that at sub-barrier energies the reaction cross section gradually increases from ^{11}B to ^{6}Li, due to the reduction of the breakup threshold energy of the projectiles.

VI. SUMMARY AND CONCLUSIONS

In the present work we have carried out the simultaneous measurement of the quasi-elastic scattering and transfer angular distributions in ^{10,11}B + ^{232}Th systems for bombarding energies from 10% below to 20% above the Coulomb barrier. Optical model analysis of the experimental data have been performed to determine both the real and the imaginary parts of the optical potential as a function of beam energy. It is observed that as the bombarding energy decreases, the imaginary potential decreases and real potential increases. The behavior of the corresponding potential parameters as a function of energy is consistent with the usual threshold anomaly, confirming the tightly bound characteristics of both the projectiles, ^{10,11}B. The reaction cross section obtained from the optical model analysis show large enhancement for the ^{10}B + ^{232}Th system in comparison to the ^{11}B + ^{232}Th system at sub-barrier energies. The reduced reaction cross sections have been obtained for both ^{10,11}B + ^{232}Th reactions and compared with the reactions of other projectiles (^{6,7}Li) with ^{232}Th target. The transfer products show a bell-shaped angular distribution at energies above the Coulomb barrier and the grazing angle shifts towards back angles at sub-barrier energies.

ACKNOWLEDGMENTS

The authors thank the operating staff of the BARC-TIFR Pelletron facility, Mumbai, for the excellent operation of the machine during the experiment. S.D. and S.M. acknowledge financial support from the UGC-DAE Consortium for Scientific Research, Kolkata Centre, India.

[1] G. R. Satchler, Phys. Rep. **199**, 147 (1991).
[2] A. G. Camacho, E. Aguilera, E. M. Quiroz, P. R. S. Gomes, J. Lubian, and L. F. Canto, Nucl. Phys. A **833**, 156 (2010).
[3] D. Patel, S. Mukherjee, D. C. Biswas, B. K. Nayak, Y. K. Gupta, L. S. Danu, S. Santra, and E. T. Mirgule, Phys. Rev. C **91**, 054614 (2015).
[4] M. A. Nagarajan, C. C. Mahaux, and G. R. Satchler, Phys. Rev. Lett. **54**, 1136 (1985).
[5] A. M. M. Maciel, P. R. S. Gomes, J. Lubian, R. M. Anjos, R. Cabezas, G. M. Santos, C. Muri, S. B. Moraes, R. L. Neto, N. Added *et al.*, Phys. Rev. C **59**, 2103 (1999).
[6] L. Fimiani, J. M. Figueira, G. V. Marti, J. E. Testoni, A. J. Pacheco, W. H. Z. Cardenas, A. Arazi, O. A. Capurro, M. A. Cardona, P. Carnelli *et al.*, Phys. Rev. C **86**, 044607 (2012).
[7] N. Keeley, S. J. Bennett, N. M. Clarke, B. R. Fulton, G. Tungate, P. V. Drumm, M. A. Nagarajan, and J. S. Lilley, Nucl. Phys. A **571**, 326 (1994).
[8] D. Abriola, A. A. Sonzogni, M. di Tada, A. Etchegoyen, M. C. Etchegoyen, J. O. F. Niello, S. Gil, A. O. Macchiavelli, A. J. Pacheco, R. Piegaia *et al.*, Phys. Rev. C **46**, 244 (1992).
[9] F. A. Souza, L. A. S. Leal, N. Carlin, M. G. Munhoz, R. Liguori Neto, M. M. de Moura, A. A. P. Suaide, E. M. Szanto, A. Szanto de Toledo, and J. Takahashi, Phys. Rev. C **75**, 044601 (2007).
[10] D. Patel, S. Santra, S. Mukherjee, B. K. Nayak, P. K. Rath, V. V. Parkar, and R. K. Choudhury, Pramana J. Phys. **81**, 587 (2013).
[11] P. Singh, S. Kailas, A. Chatterjee, S. S. Kerekatte, A. Navin, A. Nijasure, and B. John, Nucl. Phys. A **555**, 606 (1993).

[12] B. R. Fulton, D. W. Banes, J. S. Lilley, M. A. Nagarajan, and I. J. Thompson, Phys. Lett. B. **162**, 55 (1985).
[13] D. Abriola, D. DiGregorio, J. E. Testoni, A. Etchegoyen, M. C. Etchegoyen, J. O. F. Niello, A. M. J. Ferrero, S. Gil, A. O. Macchiavelli, A. J. Pacheco *et al.*, Phys. Rev. C **39**, 546 (1989).
[14] A. Shrivastava, S. Kailas, P. Singh, A. Chatterjee, A. Navin, A. M. Samant, V. R. Raj, S. Mandal, and S. K. Datta, Nucl. Phys. A **635**, 411 (1998).
[15] S. Y. Lee and W. Y. So, Eur. Phys. J. A **43**, 121 (2010).
[16] P. R. S. Gomes, I. Padron, J. O. F. Niello, G. V. Marti, M. D. Rodriguez, O. A. Capurro, A. J. Pacheco, J. E. Testoni, A. Arazi, J. Lubian *et al.*, J Phys. G **31**, S1669 (2005).
[17] M. S. Hussein, P. R. S. Gomes, J. Lubian, and L. C. Chamon, Phys. Rev. C **73**, 044610 (2006).
[18] J. M. Figueira, J. O. F. Niello, A. Arazi, O. A. Capurro, P. Carnelli, L. Fimiani, G. V. Marti, D. M. Heimann, A. E. Negri, A. J. Pacheco *et al.*, Phys. Rev. C **81**, 024613 (2010).
[19] S. Dubey, S. Mukherjee, D. C. Biswas, B. K. Nayak, D. Patel, G. K. Prajapati, Y. K. Gupta, B. N. Joshi, L. S. Danu, S. Mukhopadhyay *et al.*, Phys. Rev. C **89**, 014610 (2014).
[20] A. Gómez Camacho, N. Yu, H. Q. Zhang, P. R. S. Gomes, H. M. Jia, J. Lubian, and C. J. Lin, Phys. Rev. C **91**, 044610 (2015).
[21] Y. Y. Yang *et al.*, Phys. Rev. C **90**, 014606 (2014).
[22] H. Leucker, K. Becker, K. Blatt, W. Korsch, W. Luck, H. G. Volk, D. Fick, R. Butsch, H. J. Jansch, H. Reich, and Z. Moroz, Phys. Lett. B **223**, 277 (1989).
[23] D. C. Biswas, R. K. Choudhury, D. M. Nadkarni, and V. S. Ramamurthy, Phys. Rev. C **52**, R2827 (1995).
[24] D. C. Biswas, P. Roy, Y. Gupta, B. N. Joshi, B. Nayak, L. Danu, B. V. John, R. Vind, N. Deshmukh, S. Mukherjee *et al.*, J. Phys.: Conf. Ser. **381**, 012091 (2012).
[25] D. C. Biswas, R. K. Choudhury, B. K. Nayak, D. M. Nadkarni, and V. S. Ramamurthy, Phys. Rev. C **56**, 1926 (1997).
[26] N. Majumdar, P. Bhattacharya, D. C. Biswas, R. K. Choudhury, D. M. Nadkarni, and A. Saxena, Phys. Rev. Lett. **77**, 5027 (1996).
[27] J. Raynal, Phys. Rev. C **23**, 2571 (1981).
[28] S. Dubey, S. Mukherjee, D. Patel, Y. K. Gupta, L. S. Danu, B. N. Joshi, G. K. Prajapati, S. Mukhopadhyay, B. V. John, B. K. Nayak *et al.*, EPJ Web Conf. **86**, 00008 (2015).
[29] N. N. Deshmukh, S. Mukherjee, D. Patel, N. L. Singh, P. K. Rath, B. K. Nayak, D. C. Biswas, S. Santra, E. T. Mirgule, L. S. Danu *et al.*, Phys. Rev. C **83**, 024607 (2011).
[30] C. Mahaux, H. Ngo, and G. R. Satchler, Nucl. Phys. A **449**, 354 (1986).
[31] M. M. Gonzlez and M. E. Brandan, Nucl. Phys. A **693**, 603 (2001).
[32] Y. K. Gupta, D. C. Biswas, Bency John, B. K. Nayak, A. Chatterjee, and R. K. Choudhury, Phys. Rev. C **86**, 014615 (2012).
[33] P. R. S. Gomes, J. Lubian, I. Padron, and R. M. Anjos, Phys. Rev. C **71**, 017601 (2005).
[34] N. N. Deshmukh, S. Mukherjee, B. Nayak, D. Biswas, S. Santra, E. Mirgule, S. Appannababu, D. Patel, A. Saxena, R. Choudhury *et al.*, Eur. Phys. J. A **47**, 118 (2011).
[35] S. Mukherjee, N. N. Deshmukh, V. Guimaraes, J. Lubian, P. R. S. Gomes, A. Barioni, S. Appannababu, C. C. Lopes, E. N. Cardozo, and K. C. C. Pires, Eur. Phys. J. A **45**, 23 (2010).
[36] C. S. Palshetkar, S. Santra, A. Chatterjee, K. Ramachandran, S. Thakur, S. K. Pandit, K. Mahata, A. Shrivastava, V. V. Parkar, and V. Nanal, Phys. Rev. C **82**, 044608 (2010).